Electronic Supplementary Material (ESI) for Energy & Environmental Science.

Electronic Supplementary Information (ESI) for

A General Route via Formamide Condensation to Prepare Atomically Dispersed Metal-Nitrogen-Carbon Electrocatalysts for Energy Technologies

Guoxin Zhang,†[a,b] Yin Jia,†[a, c] Cong Zhang,[a] Xuya Xiong,[a] Kai Sun,[a, c] Ruida Chen,[a, c] Wenxing Chen,[d] Yun Kuang,[a,e] Lirong Zheng,[f] Haolin Tang,[g] Wen Liu,*[a] Junfeng Liu,*[a] Xiaoming Sun,*[a, b, c] Wen-Feng Lin[h] and Hongjie Dai[e]

[a.] State Key Laboratory of Chemical Resource Engineering, Beijing University of Chemical Technology, Beijing, China 100029;

[b.] Shandong University of Science and Technology, Electrical Engineering and Automation, Tsingtao, China 266590;

[c.] College of energy, Beijing Advanced Innovation Center for Soft Matter Science and Engineering, Beijing University of Chemical Technology, Beijing, China, 100029;

[d.] Department of Materials, Beijing Institute of Technology, Beijing, China, 100081;

[e.] Department of Chemistry, Stanford University, Stanford, CA, USA, 94305-5080

[f.] Beijing Synchrotron Radiation Facility, Institute of High Energy Physics, Chinese Academy of Sciences, Beijing, China 100049.

[g.] State Key Laboratory of Advanced Technology for Materials Synthesis and Processing, Wuhan University of Technology, Wuhan, China, 430070.

[h.] Department of Chemical Engineering, Loughborough University, Loughborough, Leicestershire, LE11 3TU, U.K.

† These authors contributed equally: Guoxin Zhang and Yin Jia.

Correspondence and requests for materials should be addressed to Wen Liu (wenliu@mail.buct.edu.cn), Junfeng Liu (ljf@mail.buct.edu.cn) or Xiaoming Sun (sunxm@mail.buct.edu.cn).

Methods

Reagents. Formamide (FA, A.R. grade) was purchased from Xilong Chemical Co., Ltd. Manganese chloride ($MnCl_2$, A.R. grade), nickel nitrate hexahydrate ($Ni(NO_3)_2 \cdot 6H_2O$, A.R. grade), zinc chloride ($ZnCl_2$, A.R. grade), cobalt nitrate hexahydrate ($Co(NO_3)_2 \cdot 6H_2O$, A.R. grade), and ferric citrate (A.R. grade) were purchased from Tianjin Fuchen Chemical Research Factory. Ethanol (purity>95%), $NH_3 \cdot H_2O$ (25~28 wt.%), N,N-dimethylformamide (DMF, purity>99.5%) was purchased from Beijing Chemical Works. Sulfuric acid (H_2SO_4, 95~98 wt.%), and nitric acid (HNO_3, 65 wt.%) were purchased from Sinopharm Chemical Reagent Co., Ltd. Carbon nanotube (CNT, purity>99.0%), active carbon (AC, purity>95.0%) and graphene oxide (GO, purity>99%) were purchased from Nanjing Xianfeng Nanomaterial Technology Co., LTD. Iridium chloride ($IrCl_3$, purity>99.8%), molybdenum chloride ($MoCl_5$, purity>99%), and tetraethyl orthosilicate (TEOS, A.R. grade) were purchased from Aladdin Reagent Co., LTD (Shanghai). The commercial Pt/C catalyst (20 wt.%, ~3 nm Pt nanoparticles on Vulcan XC-72 carbon support) and Nafion/water or ethanol solution (~5 wt.%) were purchased from Sigma-Aldrich Co., LTD. All chemicals were used as received without further purification.

Sample preparations

Synthesis of formamide-converted nitrogen-doped carbon materials (f-NC). f-NC was prepared under solvothermal conditions. Typically, 30.0 mL of FA was placed into a 40 mL Teflon-lined autoclave, sealed, and heated at 180 °C for 12 h. As-formed black product was centrifuged and purified using deionized water for 3 times, and eventually dried at 60 °C overnight.

Synthesis of formamide-converted transition metal-NC materials at low temperature (180 °C). In a typical synthesis process for atomically dispersed f-CoNC, 0.087 g $Co(NO_3)_2 \cdot 6H_2O$ were added into 30 mL FA under sonication for 0.5 h to obtain a homogeneous solution of 0.01 mol L^{-1}. Then the Co^{2+}/FA solution was transferred into a 40 mL Teflon-lined autoclave and heated at 180 °C for 12 h. Resulted black product was purified with deionized water for 3 times and dried at 60 °C overnight. For the synthesis of other types of atomically dispersed f-MNC materials including single-metal, bi-metal, and tri-metal f-MNC materials, the procedures copied the protocol of f-CoNC but simply changed the metal sources to other M salt (s) (M= Fe^{2+}, Mn^{2+}, Ni^{2+}, Zn^{2+}, Mo^{5+}, or Ir^{3+}). The synthesis of bimetal f-ZnCoNC and f-ZnFeNC followed the protocol of f-CoNC but was conducted with doubled Co or Fe dosage and additional use of 0.408 g $ZnCl_2$. Similarly, the synthesis of tri-metal f-ZnFeCoNC was conducted with0.087 g $Co(NO_3)_2 \cdot 6H_2O$, 0.100 g $Fe(Ctr)_2 \cdot 5H_2O$, and 0.408 g $ZnCl_2$.

Synthesis of f-MNC on substrates. Typical synthesis of substrate-supported f-MNC composite was demonstrated by solvothermal treatment of Co^{2+}/FA solution with the addition of GO substrate. 100.0 mg GO was initially suspended in 30.0 mL FA under sonication for 0.5 h, followed by the addition of 0.087 g $Co(NO_3)_2 \cdot 6H_2O$ under sonication for another 0.5 h to form a homogeneous solution containing 0.01 mol L^{-1} Co^{2+}. Then the Co^{2+}/GO/FA suspension was transferred into a 40 mL Teflon-lined autoclave, heated at 180 °C for 12 h. The as-obtained black product was membrane-filtered and purified with deionized water for 3 times, and freeze-dried overnight. Similarly, 100.0 mg mildly oxidized CNT, activated carbon, and SiO_2 nanosphere were used as substrates to support f-FeNC, f-NiNC, f-MnNC, and f-ZnNC layers, respectively. Resulted products were termed with respect to the metal and the substrate used. For instance, using oxidized CNT to support f-FeNC lead to the formation of CNT@f-FeNC. For the synthesis of all supported f-MNC composites, the metal concentration was kept at 0.01 mol L^{-1}. The mildly oxidized CNT, named as O_xCNT was obtained by adding 500.0 mg MWCNT into mixed HNO_3 (15.0 mL, ~65 wt.%) / H_2SO_4 (45.0 mL, ~98 wt.%) solution, and then stirring at 75 °C for 3 h, followed by thorough washing and drying. Activated carbon was used as received. SiO_2 nanospheres were prepared via the classical Stober method[1]. Typically, 15.0 mL absolute ethanol, 5.0 mL deionized water and 0.7 mL

NH_3/H_2O solution (~28 wt.%) were mixed and stirred for 0.5 h, then 0.6 mL of TEOS was added into the mixture quickly with continuous stirring for 10 h. The SiO_2 nanospheres were centrifuged and purified with ethanol for 3 times and dried at 60 °C overnight.

Synthesis of transition f-MNC materials at high temperature (900 °C). High-temperature tolerable f-MNC was derived from f-ZnMNC, M equals to Fe, or Co, or both. The dried f-ZnMNC with atomically dispersed Zn and M was placed in the ceramic boat and heated at 900 °C for 2 h in a tube furnace under flowing Ar. During this process, Zn species would be vaporized (boiling point of bulk Zn substance is 907 °C). The black 900 °C -annealed product was collected without any post-treatment and named as f-MNC900. The synthesis for high-temperature tolerable AC-supported f-FeCoNC (named as AC@f-FeCoNC900) followed that of f-FeCoNC900 except for the addition of 100.0 mg AC before the dissolution of Zn^{2+}, Fe^{2+}, and Co^{2+} sources. After the solvothermal treatment was completed, the as-formed black precipitate was membrane-filtered, purified with deionized water for 3 times, and dried at 60 °C overnight. The dried atomically dispersed f-ZnFeCoNC materials on AC (AC@f-ZnFeCoNC) precursor was placed in the ceramic boat and heated at 900 °C for 2 h in a tube furnace under flowing Ar. The black 900 °C-annealed product was collected without any post-treatment and named as AC@f-FeCoNC900.

Materials Characterization. Morphologies and structure of as-obtained samples were conveyed using field emission scanning electron microscopy (SEM, Zeiss SUPRA 55, operated at 20 kV) and transmission electron microscopy (TEM, FEI Tecnai G2 20 STwin, operated at 200 kV). High-resolution transmission electron microscopy (HRTEM, operated at 200 kV) images were recorded using a JEOL 2100 high-resolution transmission electron microscope. Aberration-corrected high-angle annular darkfield scanning transmission electron microscope (HAADF-STEM) images and element mapping images were recorded on a JEOL JEM-ARM200F TEM/STEM with a spherical aberration corrector (operated at 200 kV). Atomic force microscopy (AFM) images were measured on a Bruker scanning probe microscope. Fourier transform infrared spectroscopy (FTIR) spectra were analyzed on a Bruker Tensor II infrared spectrometer with KBr pellets. Raman spectra were recorded on a LabRAM Aramis Raman spectrometer (HORIBA Jobin Yvon). Powder X-ray diffraction (XRD) patterns were recorded on an X-ray powder diffractometer (MeasSrv F9XDZ42) with Cu Kα (λ = 0.154 nm) radiation at a scan rate of 10 °C min^{-1} in the 2θ range from 5 to 80°. X-ray photoelectron spectroscopy (XPS) was recorded on a Thermo Electron ESCALAB250 XPS Spectrometer (X-ray Source: Al). The C1s line at 284.6 eV was utilized as a reference for the binding energies in the acquired spectra. Based on the Shirley-type background, all the high-resolution XPS spectra were deconvoluted via the peak components represented by an 80% Gaussian-20% Lorentzian function.

X-ray absorption fine structure (XAFS) measurement and data analysis: XAFS spectra at the Co K-edge and Fe K-edge were measured at the beamline 1W1B station of the Institute of high energy physics (Chinese academy of sciences, China). The Co K-edge XANES data of f-CoNC, f-CoNC900 and f-FeCoNC900 were recorded in a fluorescence mode and the references (CoO and Co foil) were recorded in a transmission mode. The Fe K-edge XANES data of CNT@f-FeNC, f-FeNC, f-FeNC900 and f-FeCoNC900 were recorded in a fluorescence mode and the references (Fe_2O_3 and Fe foil) were recorded in a transmission mode. The Zn K-edge XANES data of f-ZnNC was recorded in a fluorescence mode and the references (Zn foil) was recorded in a transmission mode. The storage ring was operated at the energy of 2.5 GeV with an average electron current of 250 mA. The hard X-ray was monochromatized with Si (111) double-crystals. The obtained extended X-ray absorption fine structure (EXAFS) data were processed with the ATHENA module. The k^3-weighted EXAFS spectra in the k-space ranging from 2–10.5 $Å^{-1}$ were Fourier-transformed to real (R) space using a hanning windows.

Evaluation of catalysts towards oxygen reduction reaction (ORR). Initially, catalyst inks were prepared in a typical norm: 5.0 mg catalyst and 10.0 *u*L Nafion solution (5 wt.%) were added in 0.49 mL DMF, followed by ultrasonication for 0.5 h to form a homogeneous catalyst ink. For the catalyst films deposited on electrode, 5.0 *u*L of catalyst ink was uniformly dropped onto polished glassy carbon rotating ring-disk electrode (RRDE, diameter~6 mm) to form a catalyst loading of 0.177 mg cm^{-2}. Electrochemical measurements were carried out in a standard three-electrode cell using platinum electrode as counter electrode, saturated calomel electrode (SCE) as reference electrode, and different catalyst sample modified glassy carbon electrode (GCE) as working electrode. 0.1 mol L^{-1} KOH or 0.1 mol L^{-1} $HClO_4$ aqueous solution was used as electrolyte. Before ORR measurements, the O_2 gas was bubbled into the electrolyte for at least 30 mins to reach O_2 saturation. The cyclic voltammetry (CV) were collected at scan rate of 50 mV s^{-1}. Pine Modulated Speed Rotator equipped with a wavedrive10 electrochemical workstation was employed for RRDE measurements. The ORR polarization curves obtained using RRDE were collected at rotating speed of 1600 rpm with a scan rate of 5 mV s^{-1} in linear scan voltammetry. The ring electrode potential was set at 1.50 V vs. RHE. The hydrogen peroxide yield (H_2O_2%) and the transferred electron number (n) were determined by the following equations:

$$H_2O_2(\%) = 200 \times \frac{\frac{I_r}{N}}{I_d + \frac{I_r}{N}} \qquad (1)$$

$$n = 4 \times \frac{I_d}{I_d + \frac{I_r}{N}} \qquad (2)$$

Where I_d is the disk current, I_r is the ring current, and the current collection efficiency of the Pt ring (N) equals to 0.4. Electrochemical impedance spectroscopy (EIS) was conducted at open circuit voltage at a 10 mV AC amplitude from 10 mHz to 100 kHz.

Evaluation of catalysts towards carbon dioxide reduction reaction. Electrocatalytic activity of CNT@f-NiNC170 was evaluated for electrochemical CO_2 reduction reaction (CO_2RR) in CO_2 saturated 0.5 M $KHCO_3$ solution using linear scan voltammetry (LSV). Electrolyte were first bubbled with N_2 for 15 mins and then bubbled with CO_2 for 15 mins before the experiments. Electrodes were prepared by casting the catalyst-ethanol-Nafion ink (2.0 mg mL^{-1} catalysts, 1% Nafion) on carbon paper (area 1×1 cm^2) and a catalyst loading of 1.0 mg cm^{-2}. A silver/silver chloride electrode (Ag/AgCl) was used as the reference electrode, and a platinum electrode was used as the counter electrode. The CO_2RR was conducted in a gas-tight electrochemical cell at different potentials for 40 mins. The outlet gas was analyzed with an automatic injection system of double channel gas chromatography (Shimadzu 2014). The peak area was obtained using the EZChrom SI software. The electrode stability tests were carried out at -0.6 V vs RHE. The rate of product yield was based on the average rate collected in 2 hr. The Faradaic efficiency of CO production was calculated based on[2]:

$$\text{CO FE\%} = \frac{Q_{CO}}{Q_{total}} \times 100\% \qquad (3)$$

where Q_{CO} is the total number of electrons for CO production in the range of 2 hr, Q_{total} is the total number of electrons passing the electrode in 2 h.

Figures

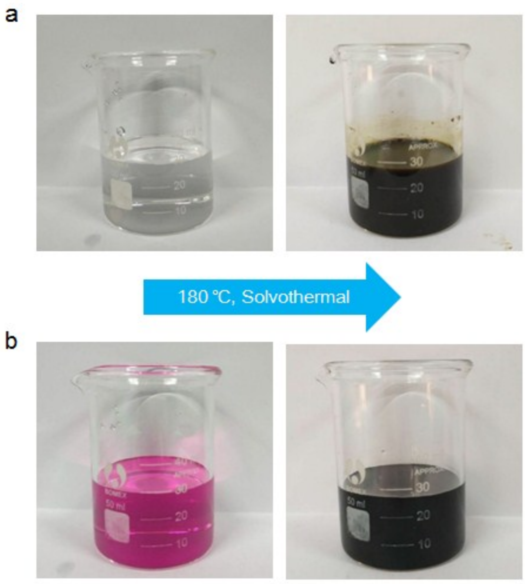

Figure S1. **Digital images of f-NC and f-CoNC.** (a) Digital images of FA solution before and after 180 °C solvothermal treatment. (b) Digital images of Co^{2+}/FA before and after 180 °C solvothermal treatment.

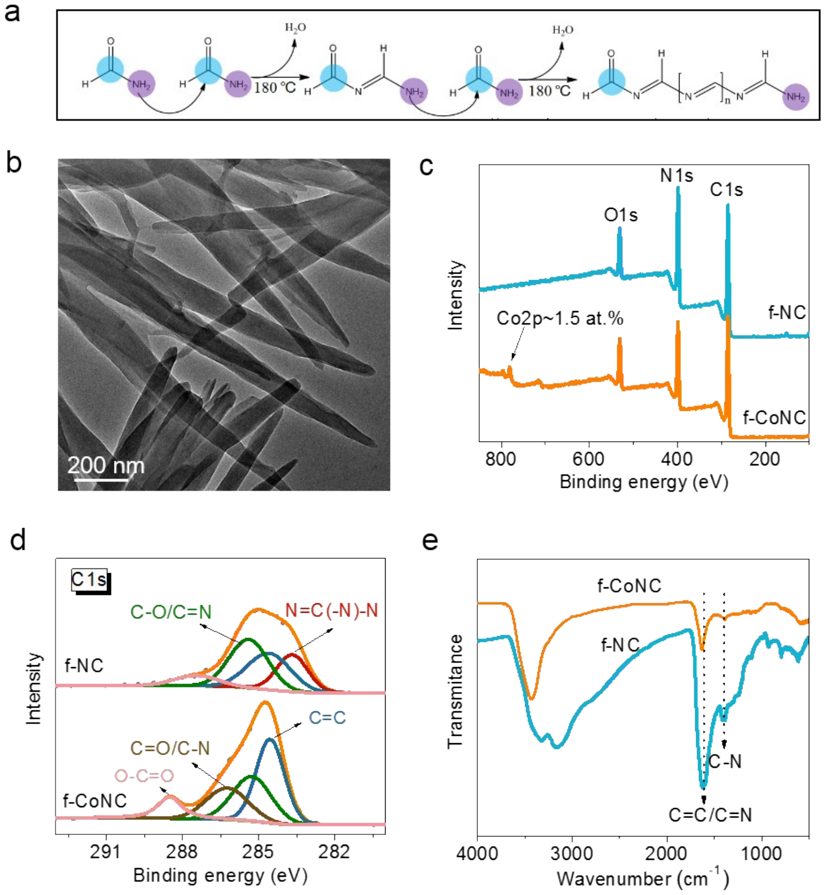

Figure S2. **Preparation scheme and characterizations for f-NC and f-CoNC.** (a) Schematic illustration of the synthetic process of f-NC. (b) TEM image of f-NC material synthesized via solvothermal treating FA at 180 °C. (c) XPS survey and (d) XPS C1s spectra of f-NC and f-CoNC. (e) FT-IR spectra of f-NC and f-CoNC.

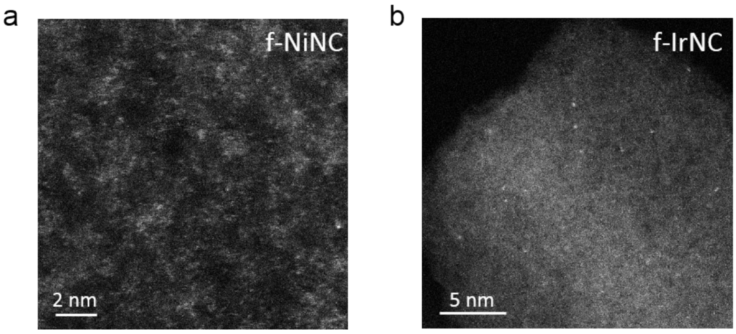

Figure S3. **HAADF-STEM images** of f-NiNC and f-IrNC.

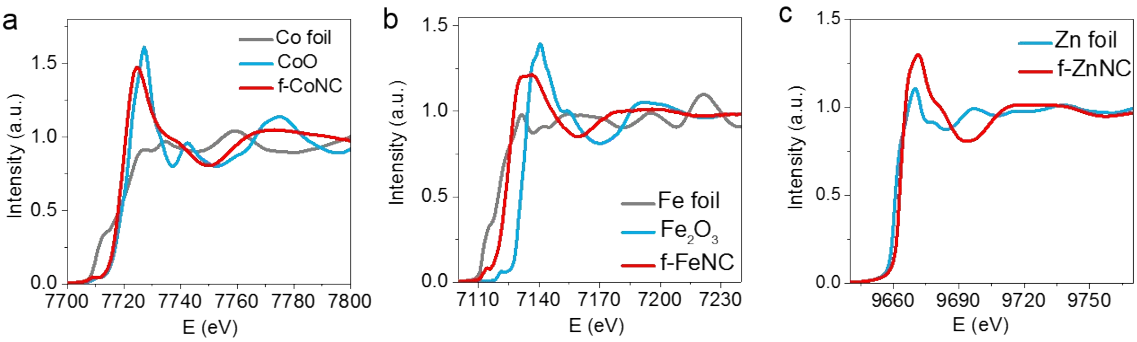

Figure S4. **Experimental K-edge XANES spectra of f-CoNC, f-FeNC and f-ZnNC.** (a) Experimental K-edge XANES Co spectra of f-CoNC and reference samples (Co foil and CoO). (b) Experimental K-edge XANES Fe spectra of f-FeNC and reference samples (Fe foil and Fe_2O_3). (c) Experimental K-edge XANES Zn spectra of f-ZnNC and reference samples (Zn foil).

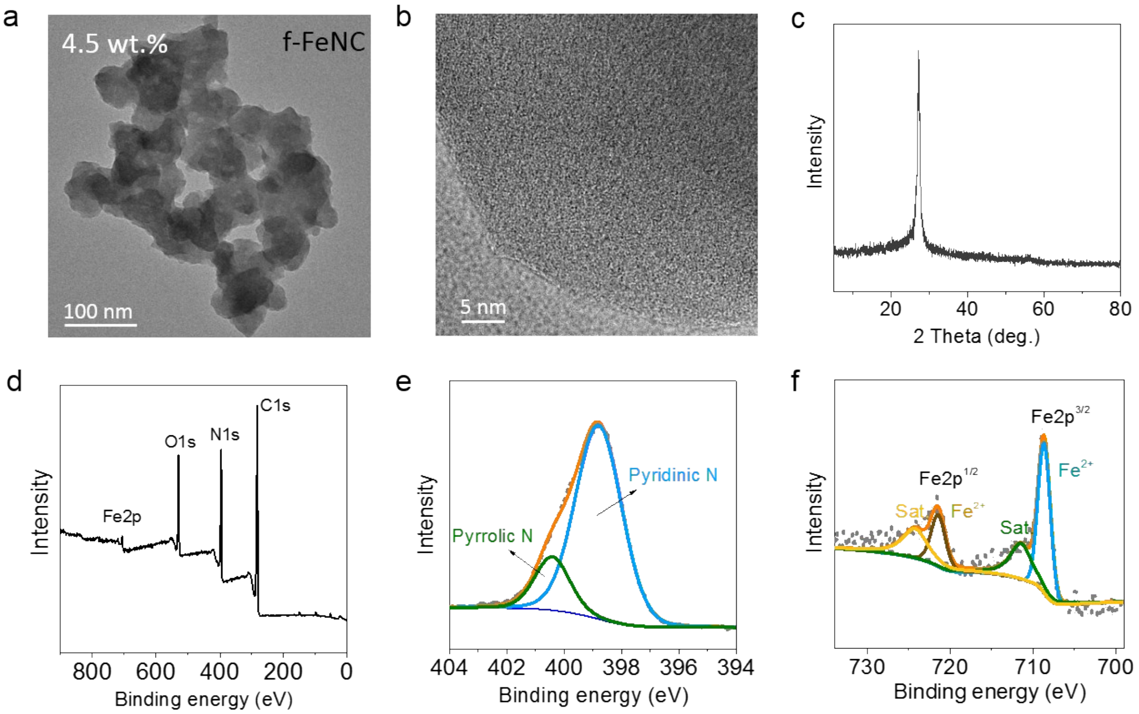

Figure S5. **Characterizations of f-FeNC.** (a) TEM image, (b) HRTEM image, (c) XRD profile, (d) XPS element survey, (e) XPS N1s spectra, and (f) XPS Fe2p spectra of f-FeNC.

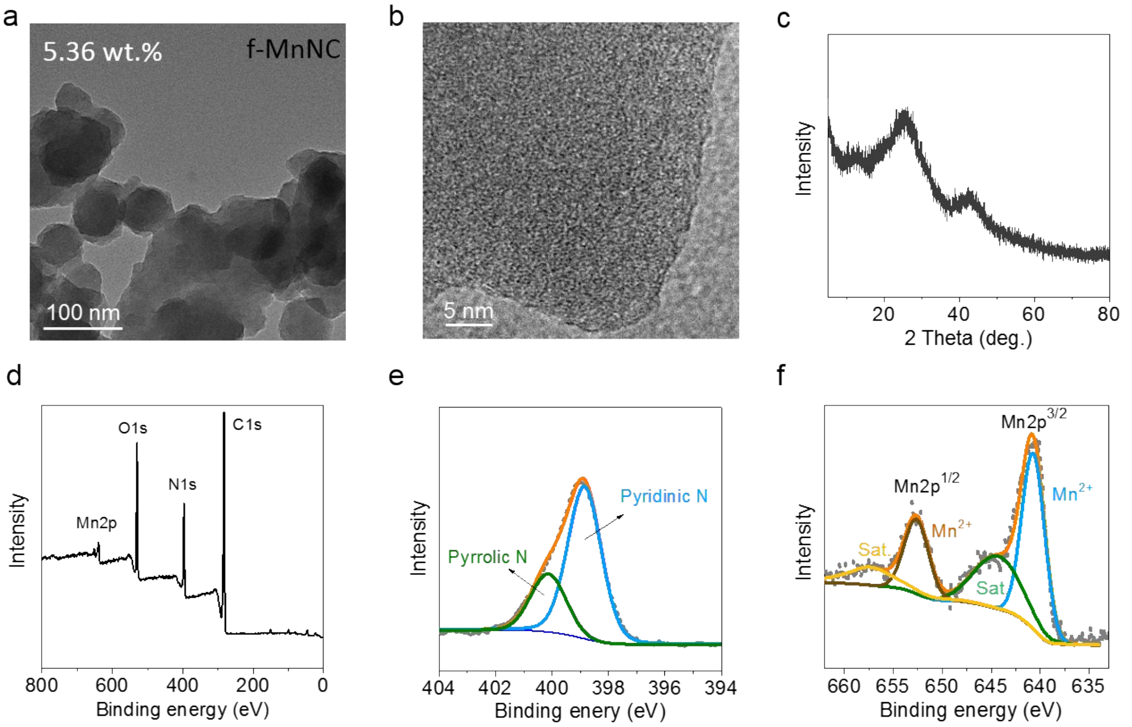

Figure S6. **Characterizations of f-MnNC.** (a) TEM image, (b) HRTEM image, (c) XRD profile, (d) XPS element survey, (e) XPS N1s spectra, and (f) XPS Mn2p spectra of f-MnNC.

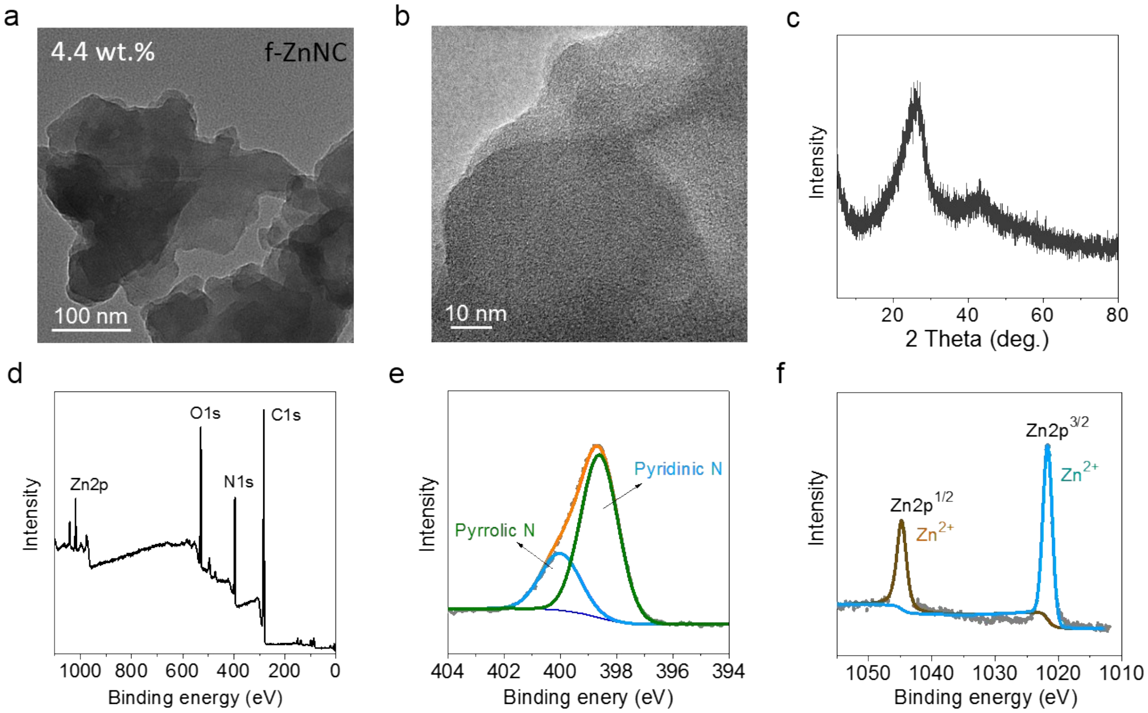

Figure S7. **Characterizations of f-ZnNC.** (a) TEM image, (b) HRTEM image, (c) XRD profile, (d) XPS element survey, (e) XPS N1s spectra, and (f) XPS Zn2p spectra of f-ZnNC.

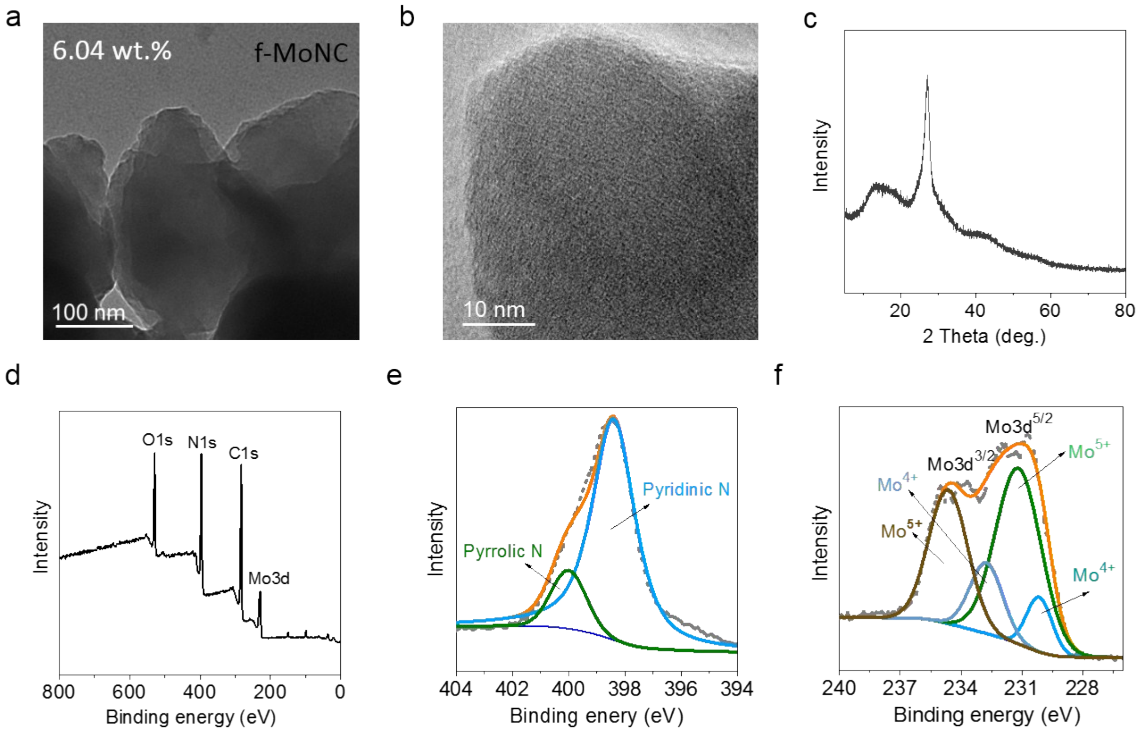

Figure S8. **Characterizations of f-MoNC.** (a) TEM image, (b) HRTEM image, (c) XRD profile, (d) XPS element survey, (e) XPS N1s spectra, and (f) XPS Mo3d spectra of f-MoNC.

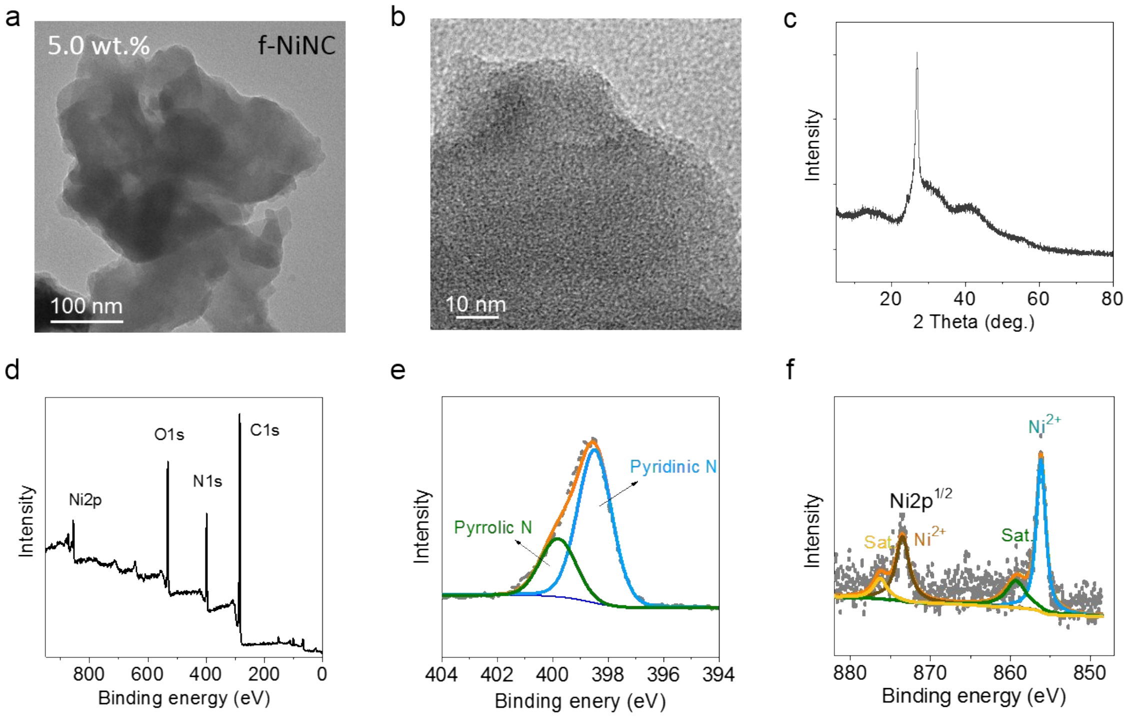

Figure S9. **Characterizations of f-NiNC.** (a) TEM image, (b) HRTEM image, (c) XRD profile, (d) XPS element survey, (e) XPS N1s spectra, and (f) XPS Ni2p spectra of **f**-NiNC.

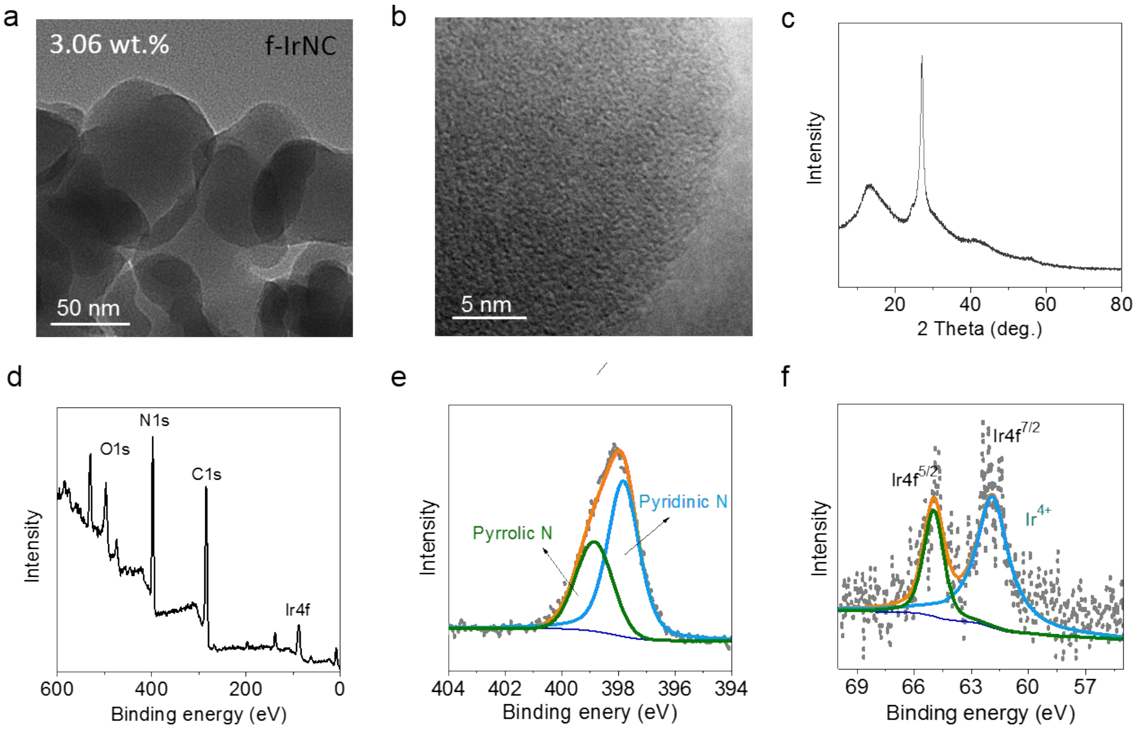

Figure S10. **Characterizations of f-IrNC.** (a) TEM image, (b) HRTEM image, (c) XRD profile, (d) XPS element survey, (e) XPS N1s spectra, and (f) XPS Ir4f spectra of f-IrNC.

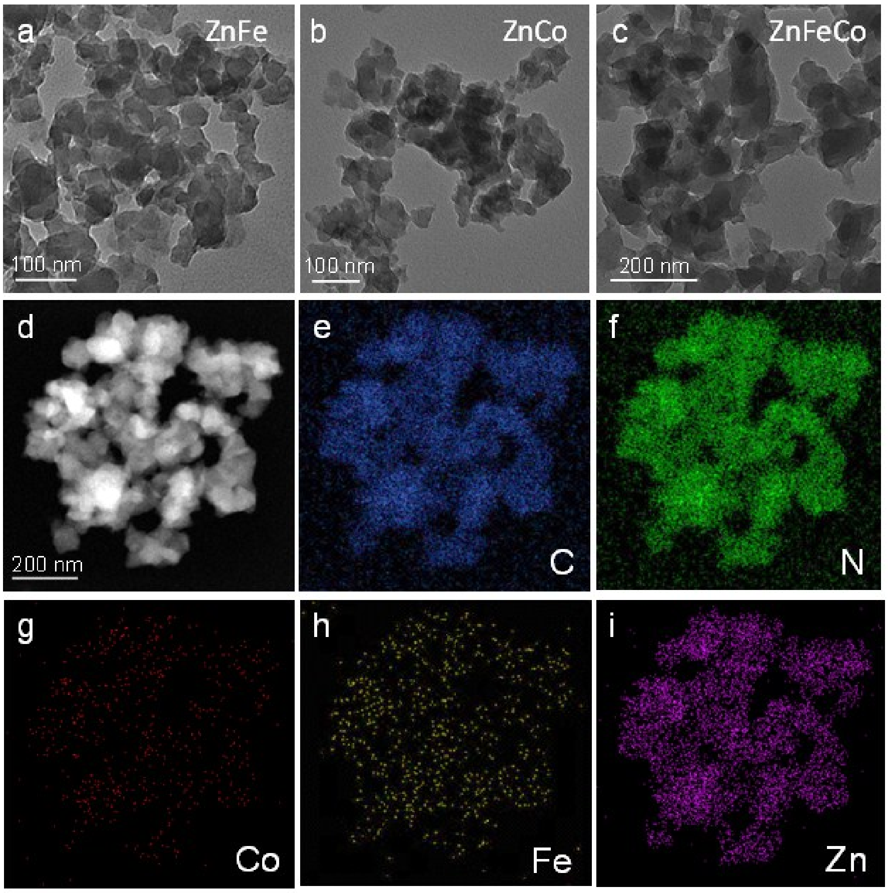

Figure S11. **Morphology characterizations of f-ZnFeNC, f-ZnCoNC and f-ZnFeCoNC.** (a)TEM images of f-ZnFeNC, (b) f-ZnCoNC, and (c) f-ZnFeCoNC. (d-i) Element mapping images of f-ZnFeCoNC, revealing the uniform distribution of C, N, Co, Fe, and Zn.

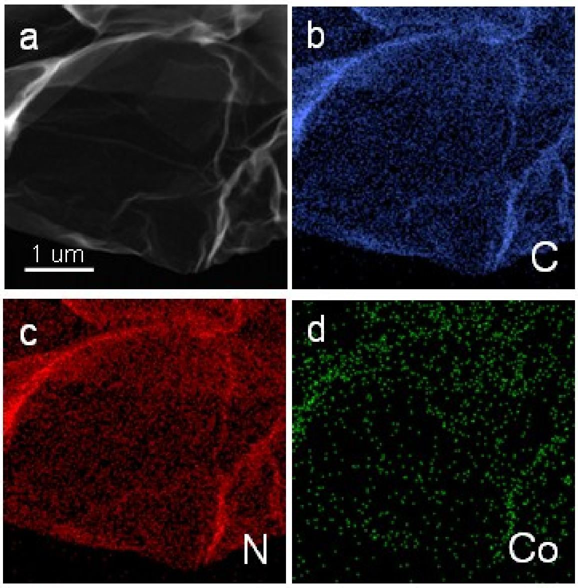

Figure S12. **Element mapping images of GO@f-CoNC**, revealing the uniform distribution of C, N, and Co.

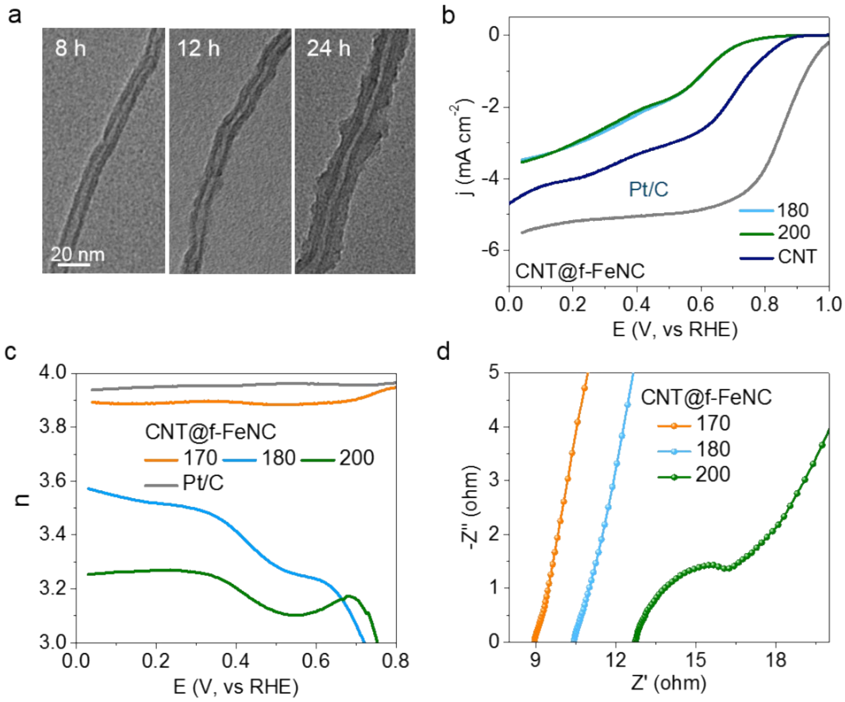

Figure S13. **Morphology characterization and electrochemical measurements on CNT@f-FeNC**. (a) TEM images of CNT@f-FeNC170 prepared with 8 h, 12 h and 24 h, respectively. (b) Linear sweep voltammogram (LSV) curves in oxygen saturated electrolyte, compared with that from commercial Pt/C catalyst, (c) Transferred electron number, and (d) EIS spectra of CNT@f-FeNC170, CNT@f-FeNC180, and CNT@f-FeNC200.

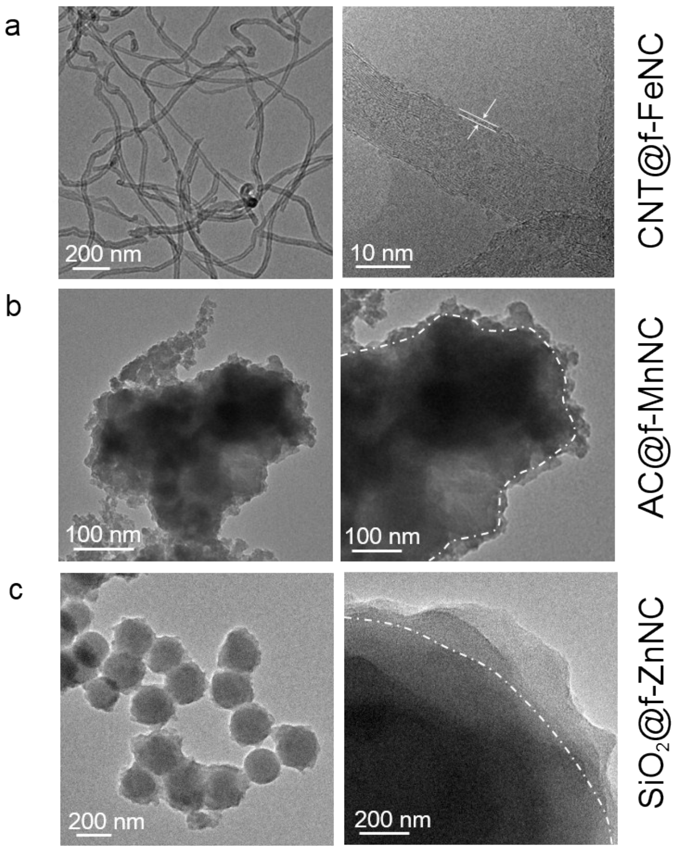

Figure S14. **Morphology characterizations.** (a) TEM and HRTEM images of CNT@f-FeNC, (b) TEM images of AC@f-MnNC. (c) TEM images of SiO_2@f-ZnNC.

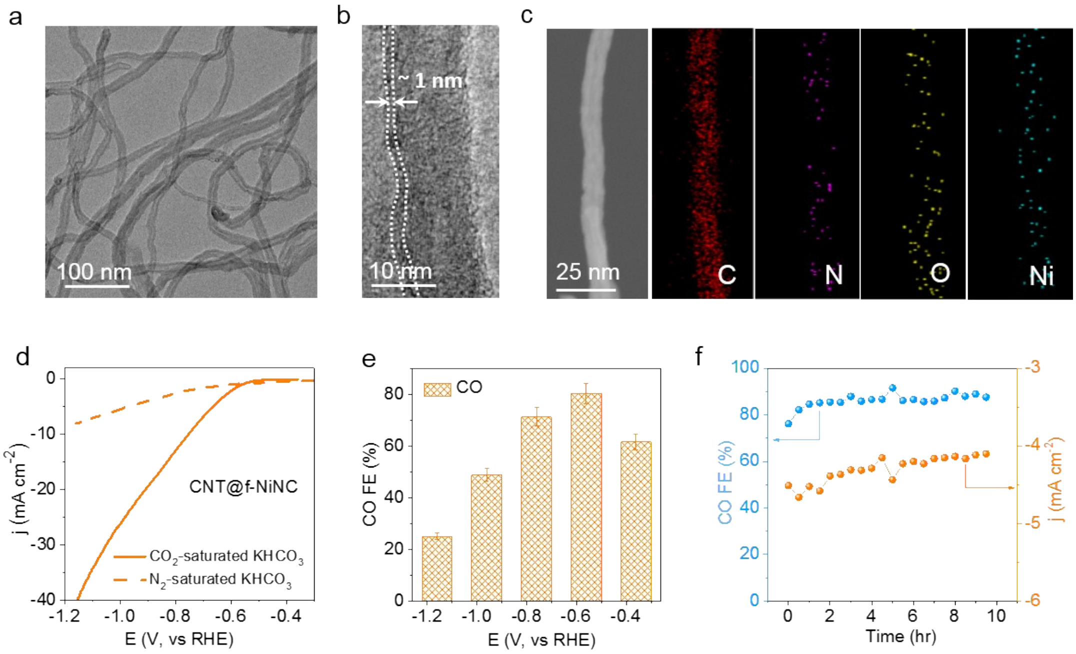

Figure S15. **Morphology characterizations and electrochemical measurements on CNT@f-NiNC**. (a) TEM image of CNT@f-NiNC170 and (b) HRTEM image of a single CNT@f-NiNC170 rod. (c) Element mapping images of CNT@f-NiNC170. (d) LSV curves of CNT@f-NiNC were performed in N_2-saturated and CO_2-saturated 0.5 M $KHCO_3$. (e) Faradaic efficiency (FE) for CO production of CO_2 reduction reaction on the CNT@f-NiNC at selected potentials. (f) Current densities and CO-yield FE of CO_2 reduction reaction on CNT@f-NiNC at -0.6 V versus RHE with 10-hour potentiostatic test.

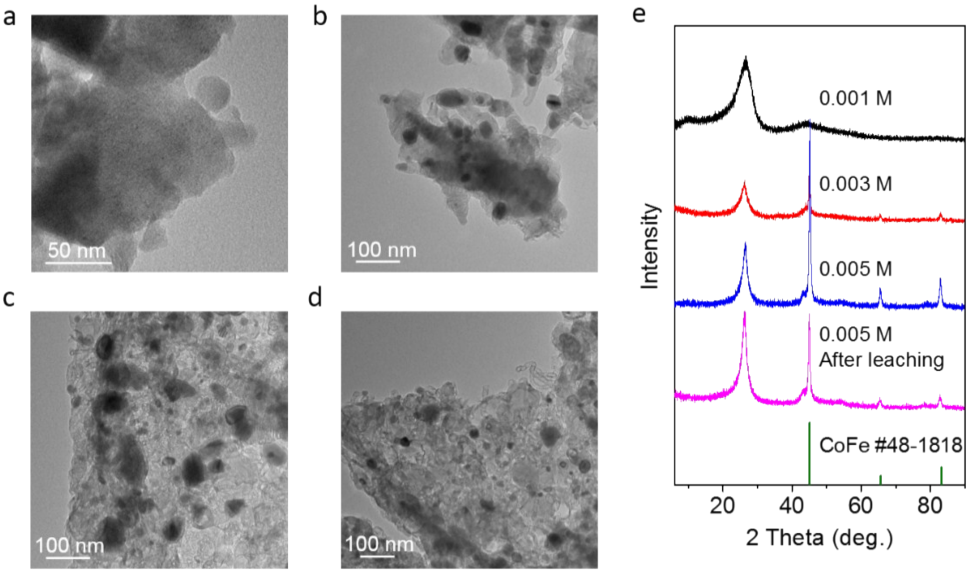

Figure S16. TEM images of f-FeCoNC900 prepared from f-FeCoNC (without Zn) with different concentrations of Co and Fe ions (a: 0.001 M, b: 0.003 M, c: 0.005 M, d: 0.005 M, after acid leaching). (e) the corresponding XRD patterns.

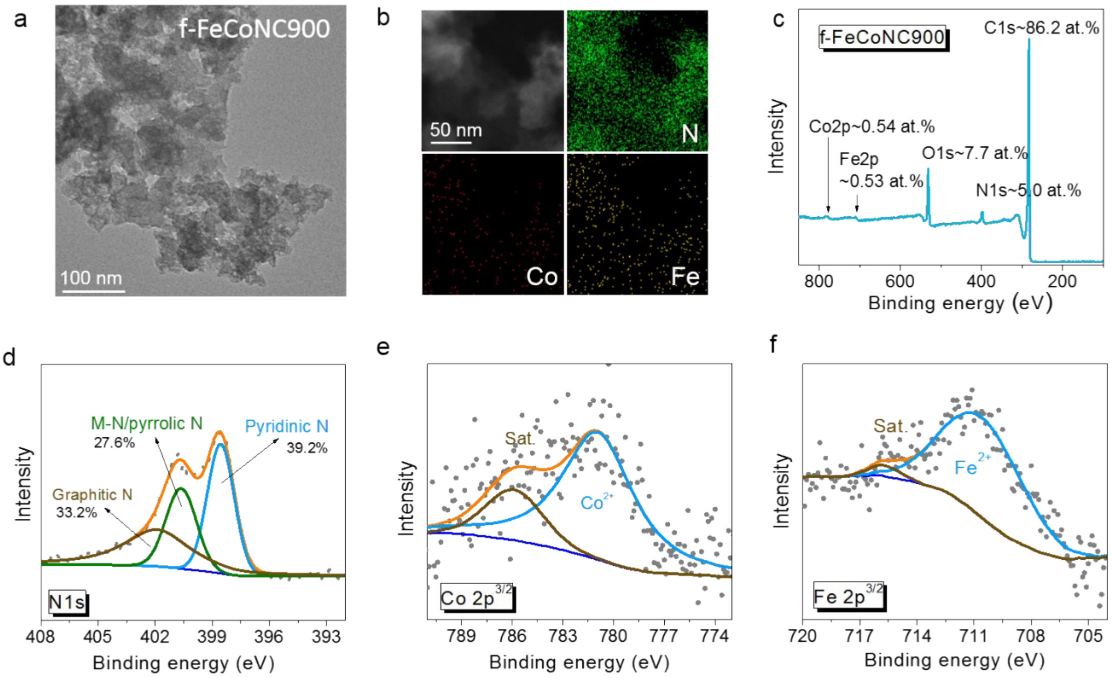

Figure S17. **Characterizations of f-FeCoNC900**. (a) HRTEM images of f-FeCoNC900, (b) Element mapping images of f-FeCoNC900, displaying the uniform distribution of atomic Fe/Co species. (c) XPS element survey, (d) N1s spectra, (e) Co2p spectra, and (f) Fe2p spectra of f-FeCoNC900.

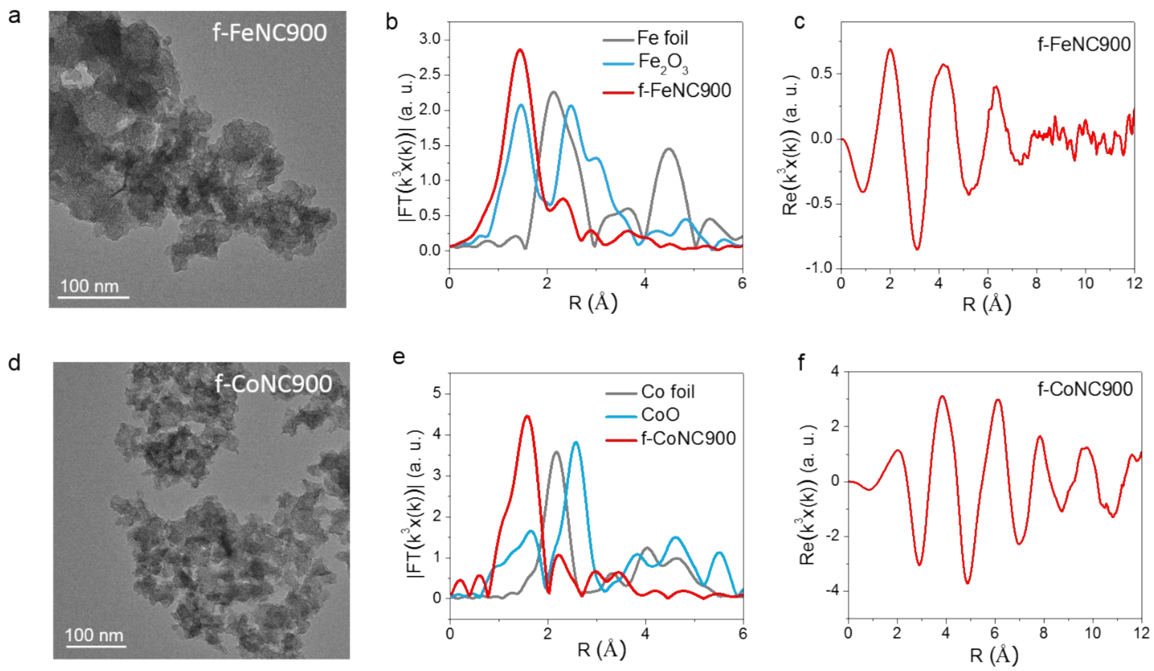

Figure S18. **Characterizations of f-FeNC900 and f-CoNC900**. (a) HRTEM images of f-FeNC900. (b, c) Fe K-edge EXAFS analysis of f-FeNC900 in R and k spaces. (d) HRTEM images of f-CoNC900. (e, f) Co K-edge EXAFS analysis of f-CoNC900 in R and k spaces.

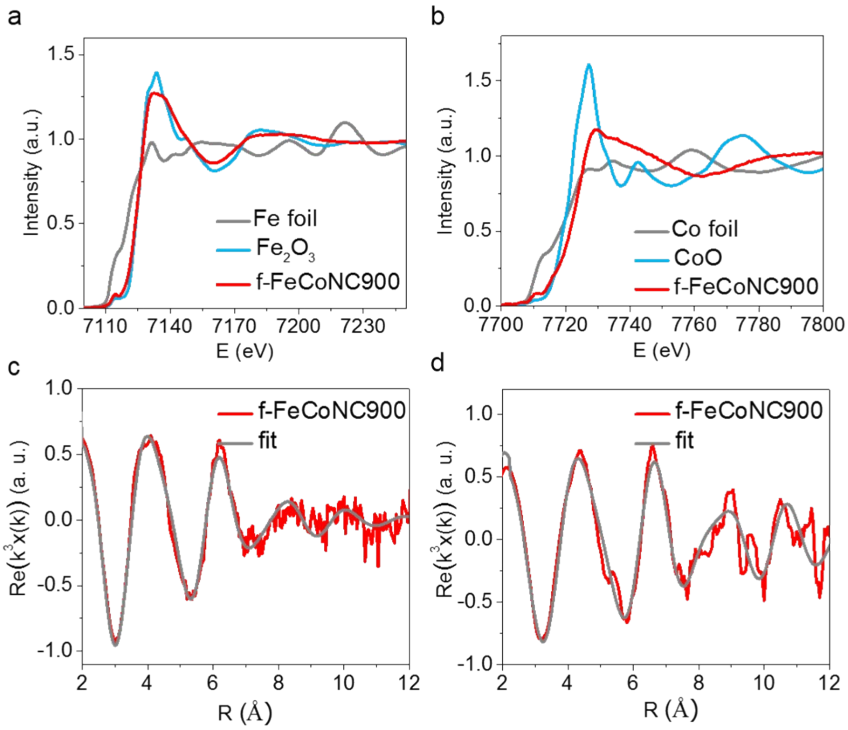

Figure S19. **Chemical state of atomically dispersed f-FeCoNC900.** (a) Experimental K-edge XANES Fe spectra of f-FeCoNC900 and reference samples (Fe foil and Fe_2O_3). (b) Experimental K-edge XANES Co spectra of f-FeCoNC900 and reference samples (Co foil and CoO). (c) The corresponding Fe K-edge and (d) Co K-edge EXAFS fitting curves of f-FeCoNC900 in k space.

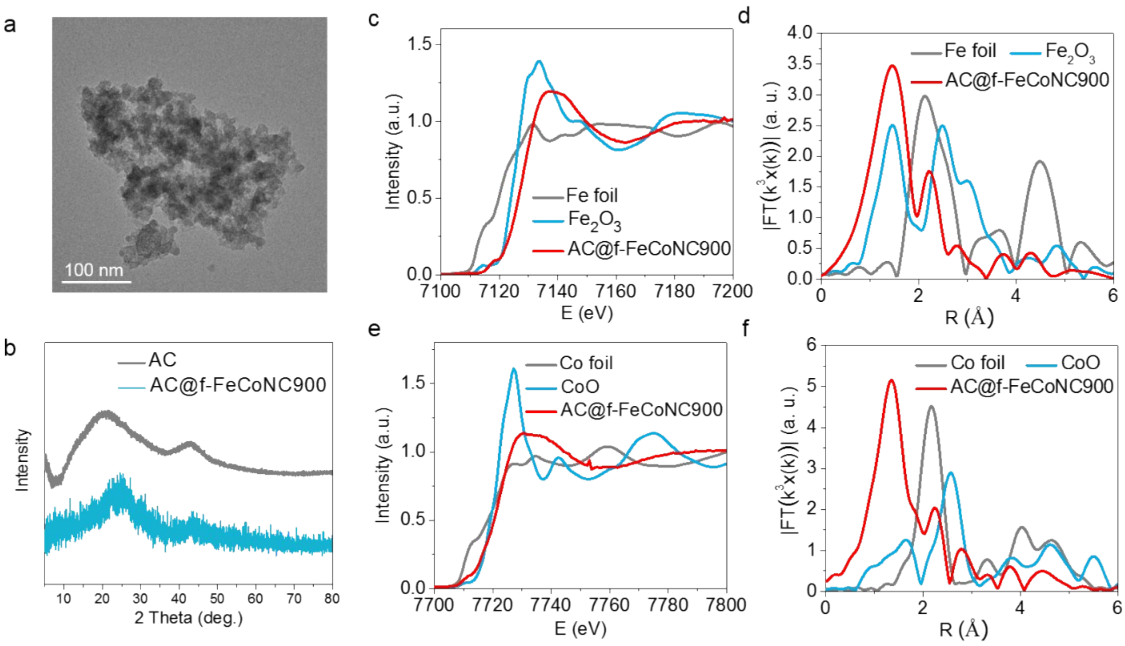

Figure S20. **Characterizations of AC@f-FeCoNC900**. (a) HRTEM image of AC@f-FeCoNC900. (b) XRD profiles of AC and AC@f-FeCoNC900. (c) Experimental K-edge XANES Fe spectra of AC@f-FeCoNC900, and reference samples (Fe foil and Fe_2O_3). (d) Fe K-edge EXAFS analysis of AC@f-FeCoNC900, and reference samples. (e) Experimental K-edge XANES Co spectra of AC@f-FeCoNC900, and reference samples (Co foils and CoO). (f) Co K-edge EXAFS analysis of AC@f-FeCoNC900, and reference samples.

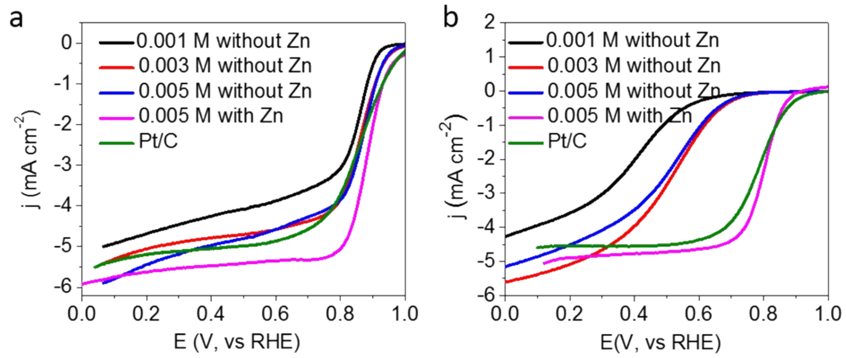

Figure S21**.** LSV curves of f-FeCoNC900 prepared from f-FeCoNC containing different concentrations of Co and Fe ions in O_2-saturated (a) 0.1 M KOH and (b) 0.1 M $HClO_4$.

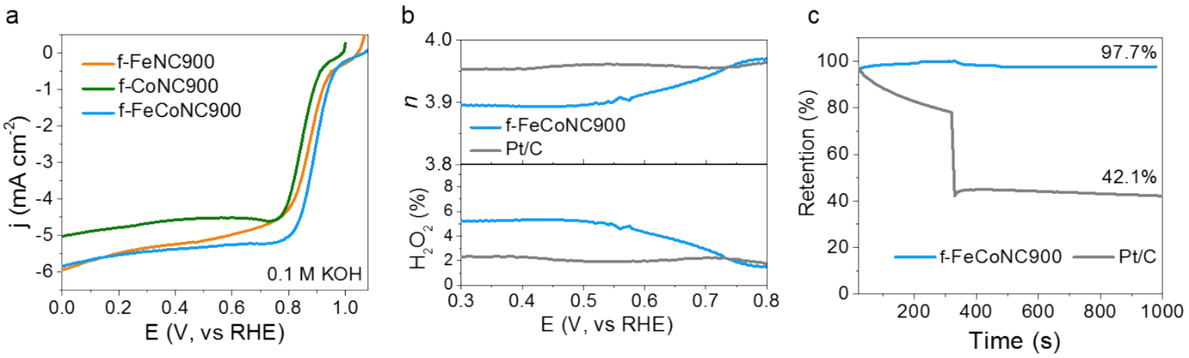

Figure S22. **Electrochemical measurements for the oxygen reduction reaction (ORR) on atomically dispersed f-FeNC900, f-CoNC900 and f-FeCoNC900 in O_2 saturated 0.1 M KOH.** (a) Polarization curves and (b) transferred electron number/generated H_2O_2 percentage of f-FeCoNC900 and Pt/C promoted ORR. (c) crossover effect tests of f-FeCoNC900 and Pt/C, 3 mL methanol was added at ~300 s.

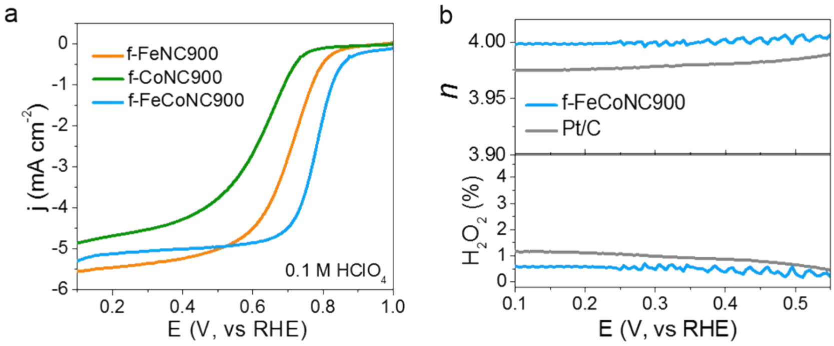

Figure S23. **Electrochemical measurements for the oxygen reduction reaction (ORR) on atomically dispersed f-FeNC900, f-CoNC900 and f-FeCoNC900** in O_2 saturated 0.1 M $HClO_4$**.** (a) Polarization curves and (b) transferred electron number/generated H_2O_2 percentage of f-FeCoNC900 and Pt/C promoted ORR.

Tables

Table S1. **Element analysis of f-NC and f-CoNC samples based on XPS characterizations**.

Sample	C	N	O	Co	Pyridinic N	Pyrrolic N	Graphitic-N
	(at. %)				(%)	(%)	(%)
f-NC	60.6	30.2	9.2	-	71.22	28.78	-
f-CoNC	63.0	25.0	10.5	1.5	74.70	25.30	-

Table S2. **Comparison of the catalytic performance toward CO_2RR of non-pyrolysis Metal N macrocyclic complexes and M-NC materials**.

Catalysts	Electrolyte	Working potential	Product & conversion efficiency	Reference
cobalt meso-tetraphenylporphyrin (CoTPP) on CNT	0.5 M $KHCO_3$ pH = 7.3	−1.35 V vs SCE	CO: 91%	3
Cobalt Porphyrin Film (Co-PP-Film)	0.5 m K_2SO_4, pH = 6.5	−1.2 V vs Ag/AgCl	CO: 84 ± 2 %	4
Co-phthalocyanine on CNT CoPc/CNT	0.1 M $KHCO_3$ pH = 6.8	-0.59 V vs RHE	CO: 92%	5
Co-phthalocyanine on CB (Carbon black) CoPc/CB	0.1 M $KHCO_3$ pH = 6.8	−0.59 V vs RHE	CO: 63%	5
Co-phthalocyanine on RGO (Reduced Graphene oxide) CoPc/RGO	0.1 M $KHCO_3$ pH = 6.8	−0.59 V vs RHE	CO: 72%	5
Fe porphyrin on carbon nanotubes (Fe-PP/CNT)	0.5 m $NaHCO_3$ pH = 7.3	-1.06 V vs SHE	CO: 85.5%	6
FeTPP-WSCAT	0.1M KCl + 0.5 M $KHCO_3$ pH = 7.3	-0.52 vs RHE	CO: 92%	7
Cobalt Porphyrin based Co-covalent organic frameworks (COF-367-Co(1%))	0.5 M $KHCO_3$ pH = 7.3	−0.67 V vs RHE	CO: 90%	8
CoPc on CFP	0.5 M $KHCO_3$ pH = 7.3	−0.8 V vs RHE	CO: 98%	9
NiPc on CFP	0.5 M $KHCO_3$ pH = 7.3	−0.8 V vs RHE	CO: 40%	9
Ni-N-C	0.1 M $KHCO_3$ pH= 6.8	−0.81 V vs RHE	CO: 82%	10
Ni SAs/N-C	0.5 M $KHCO_3$ pH = 7.3	−0.9 V vs RHE	CO: 73%	11
CNT@f-NiNC	0.5 M $KHCO_3$	−0.6 V vs RHE	CO: 84%	This work

	pH = 7.3			

Table S3. **EXAFS data fitting results of f-FeCoNC900**.

Sample	Scattering pair	CN	R(Å)	$\sigma^2(10^{-3}Å^2)$	R factor
Co in f-FeCoNC900	Co-N	2.8	1.91	3.9	0.005
	Co-Fe	0.7	2.55	6.4	
Fe in f-FeCoNC900	Fe-N	3.2	2.02	5.0	0.004
	Fe-Co	1.1	2.57	6.3	

CN is the coordination number; R is interatomic distance (the bond length between central atoms and surrounding coordination atoms); σ^2 is Debye-Waller factor (a measure of thermal and static disorder in absorber-scatterer distances). R factor is used to value the goodness of the fitting.

* This value was fixed during EXAFS fitting, based on the known structure.

Error bounds that characterize the structural parameters obtained by EXAFS spectroscopy were estimated as N ± 20%; R ± 1%; σ^2 ± 20%; ΔE_0 ± 20%.

Co-FeCo (FT range: 2.0-10.3 Å-1; fitting range: 0.6-2.8 Å)

Fe-FeCo (FT range: 2.0-10.5 Å-1; fitting range: 0.5-3.0 Å)

References

1. Y. Pan, R. Lin, Y. Chen, S. Liu, W. Zhu, X. Cao, W. Chen, K. Wu, W.-C. Cheong, Y. Wang, L. Zheng, J. Luo, Y. Lin, Y. Liu, C. Liu, J. Li, Q. Lu, X. Chen, D. Wang, Q. Peng, C. Chen and Y. Li, *J. Am. Chem. Soc.*, 2018, **140**, 4218-4221.
2. H. B. Yang, S.-F. Hung, S. Liu, K. Yuan, S. Miao, L. Zhang, X. Huang, H.-Y. Wang, W. Cai, R. Chen, J. Gao, X. Yang, W. Chen, Y. Huang, H. M. Chen, C. M. Li, T. Zhang and B. Liu, *Nat. Energy*, 2018, **3**, 140-147.
3. X. M. Hu, M. H. Ronne, S. U. Pedersen, T. Skrydstrup and K. Daasbjerg, *Angew. Chem. Int. Ed.*, 2017, **56**, 6468-6472.
4. J. E. Pander, A. Fogg and A. B. Bocarsly, *ChemCatChem*, 2016, **8**, 3536-3545.
5. X. Zhang, Z. Wu, X. Zhang, L. Li, Y. Li, H. Xu, X. Li, X. Yu, Z. Zhang, Y. Liang and H. Wang, *Nat. Commun.*, 2017, **8**, 14675.

6. A. Maurin and M. Robert, *Chem. Commun.*, 2016, **52**, 12084-12087.

7. A. Tatin, C. Comminges, B. Kokoh, C. Costentin, M. Robert and J.-M. Savéant, *Proc. Natl. Acad. Sci.*, 2016, **113**, 5526-5529.

8. S. Lin, C. S. Diercks, Y.-B. Zhang, N. Kornienko, E. M. Nichols, Y. Zhao, A. R. Paris, D. Kim, P. Yang and O. M. Yaghi, *Science*, 2015, **349**, 1208-1213.

9. Z. Zhang, J. Xiao, X. J. Chen, S. Yu, L. Yu, R. Si, Y. Wang, S. Wang, X. Meng and Y. Wang, *Angew. Chem. Int. Ed.*, 2018.

10. T. Möller, W. Ju, A. Bagger, X. Wang, F. Luo, T. Ngo Thanh, A. S. Varela, J. Rossmeisl and P. Strasser, *Energy Environ. Sci.*, 2019.

11. C. Zhao, X. Dai, T. Yao, W. Chen, X. Wang, J. Wang, J. Yang, S. Wei, Y. Wu and Y. Li, *J. Am. Chem. Soc.*, 2017, **139**, 8078-8081.